



ULTIMATE DRIFT CAPACITY FOR SLENDER RC WALLS

S. Kono⁽¹⁾, C. Netrattana⁽²⁾, H. Watanabe⁽³⁾, M. Tani⁽⁴⁾ and M. Sakashita⁽⁵⁾

⁽¹⁾ Professor, Tokyo Institute of Technology, kono.s.ae@m.titech.ac.jp

⁽²⁾ Ph.D. candidate, Tokyo Institute of Technology, chanipa.net@gmail.com

⁽³⁾ Assistant Professor, Tokyo Institute of Technology, watanabe.h.as@m.titech.ac.jp

⁽⁴⁾ Associate Professor, Kyoto University, tani@archi.kyoto-u.ac.jp

⁽⁵⁾ Research Fellow, Building Research Institute, m-saka@kenken.go.jp

Abstract

A revised edition of Standards for Structural Calculation of RC Structures was published by the Architectural Institute of Japan in 2010. It relaxed requirements on boundary columns and allows the design of rectangular section walls. However, boundary end region should be well confined so that structural walls with a rectangular section have similar seismic performance to those with boundary columns. In the meantime, the 2010 Chile Off-Maule Earthquake and the 2011 Christchurch Earthquake revealed weakness of slender RC walls which suffered flexural failures due to crushing of concrete or buckling and fracture of longitudinal reinforcement at boundary regions. Damage in two earthquakes urged the international engineering society to evaluate the ultimate drift capacity and failure modes of RC walls with higher accuracy.

In order to simulate compression controlled flexural failure, a fiber based model was constructed and calibrated using series of experimental studies conducted on reinforced concrete walls last several years in Japan. Then a parametric study was carried out with the fiber based model to simulate the hysteresis curves of walls to see effects of three variables on the load and drift level of characteristic points of a backbone curve. Three variables were concrete compressive strength (30MPa – 60MPa), confining reinforcement ratio in boundary regions (1.1% - 3.2%) and axial load ratio (0% - 50%). The parametric study showed that three variables have different degree of influences on the features of backbone curves and the axial load ratio is the most influential factor on the ultimate drift capacity.

Keywords: slender walls; ultimate drift capacity; confinement; flexural compression failure



1. Introduction

The Architectural Institute of Japan (AIJ) published a revised edition of “Standards for Structural Calculation of RC Structures” [1] in 2010. The 2010 AIJ RC Standards relaxed requirements on boundary columns which had been mandatory for structural walls higher than five-story in the 1999 AIJ RC standards [2]. The 2010 edition allows designing rectangular section walls with good confinement at boundary end regions. The boundary end region, which is supposed to act equivalently as a boundary column, should be well confined so that structural walls with a rectangular section have similar seismic performance to those with boundary columns.

It is well known that the 2010 Chile Off-Maule Earthquake and the 2011 Christchurch Earthquake caused severe damage to RC walls [3]. They suffered flexural failures due to crushing of concrete or buckling and fracture of longitudinal reinforcement at boundary regions. In order to avoid this type of damage, it is necessary to develop tools to assess the ultimate drift capacity and failure mode with higher accuracy.

Fiber based section analyses were frequently conducted by many researchers (for example Pugh et al. [4]) to provide a simple design tool for practicing engineers. One of the advantages of fiber based section analysis is its simplicity and stability. Disadvantages are ambiguity of determining equivalent plastic hinge length and non-flexural components such as shear and pull-out drift contributions [5][6]. Some advanced codes consider the shear - flexure interaction [7] or even shear - flexure - axial interaction [8] to clarify this ambiguity.

This paper shows the results of the numerical parametric analysis to understand the effects of important variables on the feature of backbone curve of RC rectangular walls. First, a fiber based numerical program was made to simulate hysteresis curves obtained from wall test data. The numerical program was calibrated using twenty-four wall specimens tested in a wall project in Japan. Then a parametric study was carried out with the fiber based program to simulate the hysteresis curves of walls to see effects of three variables on the load and drift level of characteristic points of a backbone curve. Three variables were concrete compressive strength (30MPa – 60MPa), confining reinforcement ratio in boundary regions (1.1% - 3.2%) and axial load ratio (0% - 50%). The parametric study shows that three variables have different degree of influences on the features of backbone curve and the axial load ratio is the most influential factor on the ultimate drift capacity.

2. Numerical Simulations with A Fiber Based Model

2.1. Basic concept of backbone curve modeling

To obtain a backbone curve of load (Q) – drift ratio (R) relation of RC walls, drift ratio (R) is simulated by summing the flexural drift component, R_f , and the shear drift component, R_s , as shown in Eq. (1).

$$R = R_f + R_s \quad (1)$$

It is noted that a drift component due to pullout from the stub, $R_{pullout}$, is not modelled explicitly but included in R_f for simplicity in this study. Aaleril et al. [5] modelled a drift due to flexural deformation of wall panel, $R_{f-panel}$, and a drift component due to pullout from the stub, $R_{pullout}$, together assuming that the yield penetration depth is as large as the surface plastic hinge length. With this assumption, the drift components, $R_{f-panel}$ and $R_{pullout}$, are comparable in magnitude but the experimental results by Kono et al. [9] shows that penetration depth is not that large and the drift due to pullout from the stub ranges from 10 to 20% of the total drift. This study considers R_f as one independent variable and two components of $R_{f-panel}$ and $R_{pullout}$ are not explicitly taken care of separately. In a strict sense, it may be good to model each of $R_{f-panel}$ and $R_{pullout}$ as Aaleril et al. [5] or Beyer et al. [6] indicated.

2.2. Flexural drift component and the definition of the ultimate flexural drift

The flexure drift component, R_f , in Eq. (1) is assumed to consist of elastic component, R_{fe} , and plastic component, R_{fp} , as shown in Fig. 1(a). Two components are computed based on the idealized curvature distribution in Fig. 1 (b) and their summation makes R_f as Eq. (2).

$$R_f = R_{fe} + R_{fp} = \frac{1}{H} (\Delta_{fe} + \Delta_{fp}) \tag{2}$$

where elastic drift component, $R_{fe} = \Delta_{fe}/H$, is computed from a linear elastic curvature distribution, ϕ_{fe} , over the height. The plastic drift component, $R_{fp} = \Delta_{fp}/H$, is computed from a uniform plastic curvature distribution, ϕ_{fp} , over the equivalent plastic hinge length, l_p . The plastic rotation is supposed to take place after the flexural yielding in reality but assumed to start from the beginning of loading for simplicity.

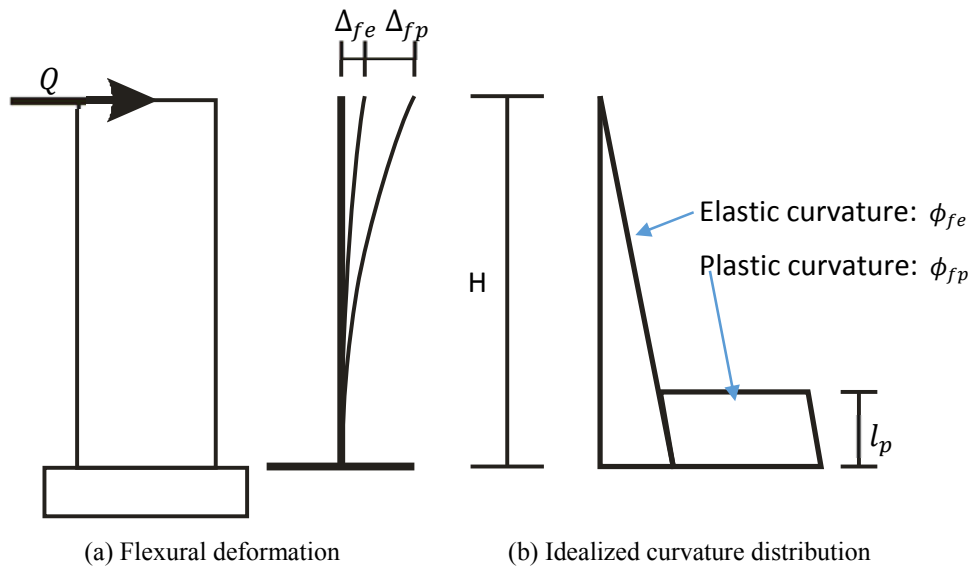
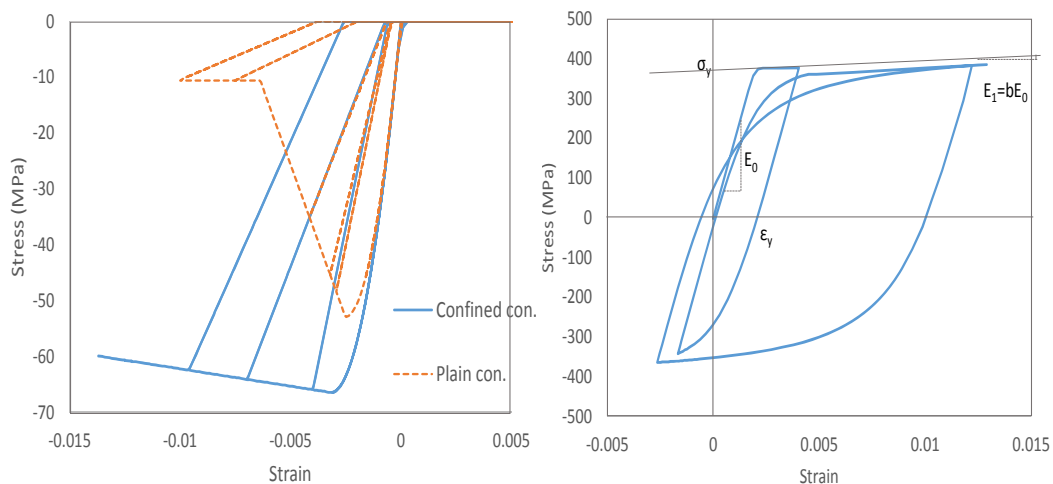


Fig. 1 – Decomposition of flexural drift component



(a) Kent and Park Model [10] for plain and confined concrete (b) Menegotto and Pinto Model [11] for reinforcement

Fig. 2 – Stress-strain models for concrete and reinforcement



A fiber based section analysis is used to compute plastic flexural drift component, Δ_{fp} . Different fibers represent elements for either plain concrete, confined concrete and vertical reinforcing bars. The stress-strain relation of plain and confined concretes is modeled with Kent and Park model [10] (Fig. 2(a)) and that of vertical reinforcing bars was modeled with Menegotto and Pinto model [11] (Fig. 2 (b)). Once a set of shear force, Q , and plastic drift component, R_{fp} , is obtained, corresponding R_{fe} can be computed using a basic elastic theory as $\Delta_{fe} = QH^3 / (3EI)$ for a cantilever type loading system in Fig. 1.

The ultimate flexural drift component, R_{uf} , is computed with Eq. (3).

$$R_{uf} = \frac{1}{H} (\Delta_{ufe} + \Delta_{ufp}) \quad (3)$$

$$\Delta_{ufp} = l_p \phi_{ufp} (H - 0.5l_p) \quad (4)$$

$$\Delta_{ufe} = \frac{Q_u H^3}{3EI} \quad (5)$$

where Δ_{ufp} is the ultimate plastic drift component, Δ_{ufe} is the elastic drift component when the plastic drift (Δ_{fp}) reaches the ultimate plastic drift (Δ_{ufp}), l_p is the effective plastic hinge length, ϕ_{ufp} is the ultimate plastic curvature over the plastic hinge, Q_u is the shear force corresponding to the ultimate plastic curvature (ϕ_{ufp}), and EI is the flexural stiffness of the wall. In numerical analysis, the ultimate drift is assumed to happen when one of following three conditions is met. In the numerical simulation, Criteria #2 governs most specimens.

1. When the load carrying capacity decreases to 80% of the peak load.
2. When the extreme compressive fiber strain of core concrete reaches the ultimate limit strain, ε_{cu} . This study uses Mander's model in Eq. (6) to determine ε_{cu} .
3. When the strain of tensile vertical reinforcing bars reaches the ultimate limit strain. This study uses 0.15.

The ultimate limit strain of confined concrete, ε_{cu} , is computed with Mander's model [12][13] as Eq. (6).

$$\varepsilon_{cu} = 0.004 + 1.4 \rho_s f_{yh} \varepsilon_m / f'_{cc} \quad (6)$$

where f'_{cc} is the compressive strength of confined concrete computed using Kent and Park model, ε_m is the steel strain of confining reinforcement at the maximum tensile stress, ρ_s and f_{yh} is the volumetric ratio and yield strength of confining steel, respectively. The value of ε_m is controversial. The original Mander's equation is derived by considering an energy balance between the core concrete and confining steel, and confined concrete is considered to reach the limit strain, ε_{cu} , when the confining steel reinforcement reaches the strain at the maximum tensile stress over the whole length. However, experimental results by Kono et al. [9] showed that the strain of steel reinforcement is far from uniform and only the limited part of steel reached the strain of the maximum tensile stress.

2.3. Shear drift component

Beyer et al.'s model [6] is used to simulate the shear drift component. This model allows the estimation of the ratio of shear-to-flexural deformations for shear walls whose shear-transfer mechanism is not significantly deteriorating. The model assumes that the ratio of shear-to-flexural drifts remains approximately constant over the entire range of imposed displacement ductility. However, the model does not function for walls whose shear transfer mechanism significantly degrades since the ratio of shear-to-flexural deformations increases. The ratio of shear drift, R_s , to flexural drift, R_f , is expressed as Eq. (7).

$$\frac{R_s}{R_f} = 1.5 \frac{\varepsilon_{mean}}{\phi H \tan \beta} \quad (7)$$



$$\beta = \tan^{-1} \left\{ \left(\frac{jd}{V} \right) \left(f_l b_w + \frac{A_{sw} f_{yw}}{s} \right) \right\} \leq 90^\circ \quad (8)$$

where ε_{mean} is the axial strain at the center of gravity of the wall section, ϕ is the curvature at the critical section, H is the shear span. Variable β is the cracking angle measured against the element axis and assumed 45 degrees in this study, which is suggested by Beyer et al. for simplification. Variables ε_{mean} and ϕ are easily derived from the fiber-type section analysis. With this equation, the shear drift component can be obtained with an easy and stable manner once the flexural drift component is computed.

2.4. Simulation procedures

Following procedures are taken to simulate backbone curves.

1. Assume a set of plastic hinge length, l_p , and the steel strain at the maximum tensile stress, ε_m .
2. For a given plastic curvature, ϕ_{fp} , compute R_{fp} and Q using a fiber based section analysis.
3. Compute R_{fe} for Q obtained in #2.
4. Compute R_f by summing R_{fe} and R_{fp} with Eq. (2).
5. Compute R_s with Eq. (7).
6. Compute drift, R , with Eq. (1).
7. Repeat from #2 through #6 to obtain $Q-R_f$ relation, $Q-R_s$ relation, and finally $Q-R$ relation until R_f reaches R_{uf} (Eq. (3)).

This fiber based numerical analysis needs to assume both equivalent plastic hinge length, l_p , and the steel strains of confining reinforcement at the maximum tensile stress, ε_m , before starting analysis. These two variables were determined by using test results of twenty-four wall specimens. The detail of this process is explained in another paper [13] and this paper briefly explains its summary. For l_p , six existing equations is used (Paulay and Priestly [13], Kowalski [16], Thomsen and Wallace [17], Takahashi et al. [18], Kabeyasawa et al. [19], Wallace and Moehle [20], Priestly and Seible [21], Panagiorakos [22], Bohl and Adebare [23]) The steel strains of confining reinforcement at the maximum tensile stress, ε_m , is taken between 1% and 8% at one percent increment (eight types). By combining six l_p 's and eight ε_m 's, some 50 combinations for l_p and ε_m were computed for each specimen and the best combination to simulate the ultimate drift was studied. Kono et al. [13] suggested three sets of l_p and ε_m to simulate the ultimate drifts for shear walls with similar precision but this study selected the best combination of three.

$$l_p = 0.33l_w \text{ and } \varepsilon_m = 2\% \quad (9)$$

where l_w is the length of wall.

3. Parametric Study to Best Simulate Backbone Curve Characteristics

3.1. Outline of parametric study to simulate backbone curves

Parametric study was carried out on rectangular RC shear walls shown in Fig. 3. The examined cross section of structural wall is 1750x128 mm with wall height of 2800 mm (Shear span to wall length ratio was 2.0). Confining area width was 350 mm (20% of wall length). It was assumed that the yield strengths of vertical reinforcement (D6 and D10) and shear reinforcement (D6) were 380MPa and 370MPa, respectively. Elements in the fiber based model are shown in Fig. 4. Yellow elements are plain concrete while blue elements are confined concrete. All elements were 10 mm thick. D10 and D6 rebars are modeled separately as red and green elements, respectively. The modulus of rupture of concrete, f_r , was based on the ACI318-14 equation $f_r = 0.62\sqrt{f'_c}$ (MPa).

The numerical work considered three important variables; compressive strength (f'_c), shear reinforcement ratio in the confined region (ρ_s) and axial load ratio (η) as shown in Table 1. Compressive strength, shear rebar ratio and axial load of a prototype specimen (Specimens #1, #6 and #10 are identical and used as a prototype) has $f'_c=30$ MPa, $\rho_s=1.6\%$ (D6@80) and $\eta=10\%$, respectively. Concrete compressive strength was varied from 30 to 60 MPa, shear reinforcement ratio from 1.1 to 3.2 %, and the axial load ratio from 0% to 50%.

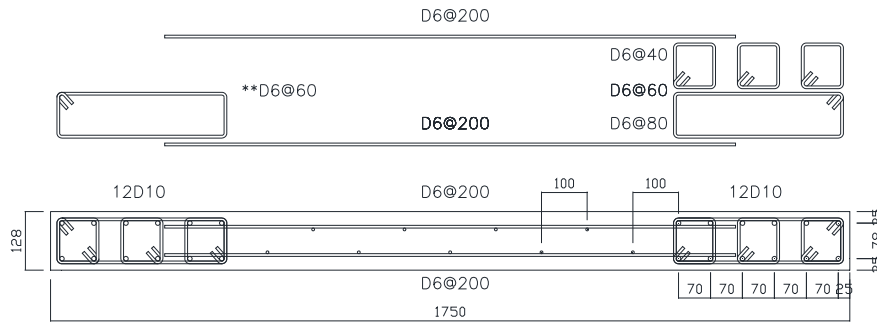


Fig. 3 – Dimensions of a specimen used in a parametric study

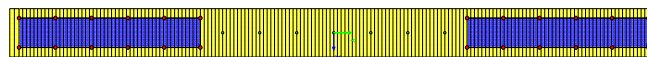


Fig. 4 – Meshed elements in the fiber based model

Table 1 – Major variables of specimens in a parametric study

Specimen #	Assumed variables					Variables for Eq. (6)	
	f'_c (MPa)	ρ_s (%)	N/Agf'_c (%)	l_p (mm)	ϵ_{sm} (%)	f'_{cc} (MPa)	ϵ_{cu}
1	30	D6@80 (1.6%)	10	578	2.0	36	0.00840
2	45					51	0.00710
3	52.5					58	0.00670
4	60					66	0.00639
5	30	D6@60 (1.1%)	10			34	0.00718
6		D6@80 (1.6%)				36	0.00840
7		D6@60 (2.1%)				37	0.00951
8		D6@40 (3.2%)				41	0.01161
9	30	D6@80 (1.6%)	0	36	0.00840		
10			10				
11			20				
12			30				
13			40				
14			50				

Specimens #1, #6 and #10 are identical.



3.2. Results and discussions

Table 2 shows the effects of concrete strength on lateral forces and drifts of four characteristic points; flexural cracking, yielding, peak and ultimate points. The lateral load – concrete strength relations and drift – concrete strength relations are plotted in Fig. 5(a) and (d), respectively. It can be seen that the compressive strength of concrete affects the load and drift of four characteristic points so slightly that the variations in load and drift are trivial. However, the increase of the compressive strength results in the increase of the peak and ultimate drifts when the compressive strength is large than 45 MPa (Fig. 5(d)).

Table 3, with Fig. 5(b) and (e), shows the effects of shear reinforcement ratio of confined region. Similar to the compressive strength of concrete, shear reinforcement ratio has minor effects on the load and drift except the peak and ultimate drifts. The increase in the peak and ultimate drifts due to confinement is larger than that due to concrete strength. For example, the ultimate drift varies from 2.41% to 2.86% when concrete strength varies from 30MPa to 60MPa. On the other hand, the ultimate drift varies from 1.80% to 2.80% when shear reinforcement ratio varies from 1.1% to 3.2%.

Table 2 – Effect of concrete strength

Specimen #	Variable	Numerical results							
	Concrete strength (MPa)	Flexural Crack		Yielding		Peak		Ultimate	
		Qcr (kN)	Rcr (%)	Qy (kN)	Ry (%)	Qmax (kN)	Rmax (%)	Qut (kN)	Rut (%)
1	30	132	0.042	305	0.17	386	2.41	386	2.41
2	45	151	0.041	340	0.20	408	2.49	408	2.49
3	52.5	158	0.041	346	0.20	414	2.62	414	2.62
4	60	164	0.043	341	0.18	423	2.86	423	2.86

Table 3 – Effect of transverse reinforcement ratio

Specimen #	Variable	Numerical results							
	ps (%)	Flexural Crack		Yielding		Peak		Ultimate	
		Qcr (kN)	Rcr (%)	Qy (kN)	Ry (%)	Qmax (kN)	Rmax (%)	Qut (kN)	Rut (%)
5	1.1	131	0.042	321	0.18	376	1.80	376	1.80
6	1.6	132	0.042	305	0.17	386	2.41	386	2.41
7	2.1	132	0.042	305	0.17	389	2.49	389	2.49
8	3.2	132	0.042	321	0.18	389	2.80	389	2.80

Table 4 – Effect of axial force ratio

Specimen #	Variable	Numerical results							
	Axial load ratio (%)	Flexural Crack		Yielding		Peak		Ultimate	
		Qcr (kN)	Rcr (%)	Qy (kN)	Ry (%)	Qmax (kN)	Rmax (%)	Qut (kN)	Rut (%)
9	0	45	0.030	187	0.16	283	4.29	283	4.29
10	10	132	0.042	305	0.17	386	2.41	386	2.41
11	20	220	0.094	446	0.21	504	0.64	485	1.36
12	30	296	0.102	565	0.24	599	0.43	536	0.84
13	40	361	0.130	629	0.25	659	0.32	520	0.60
14	50	358	0.140	666	0.30	668	0.31	405	0.54

Table 4, with Fig. 5(c) and (f), shows the effects of axial load ratio. Increase of axial load ratio results in the increase of load for four characteristic points. This effect may be easily explained from the axial force - moment capacity interaction. It is noted that the peak and ultimate drifts dramatically decrease as the axial load ratio increases. This detrimental effect of axial load ratio can be seen from lateral load – drift relations for Specimens #9 through #14 in Fig. 6. It should be noted that Fig. 6(a) and (b) have larger scale of x-axis. When axial load ratio

is less than 10% (Specimens #9 and #10), the peak load and ultimate load are identical. However, the ultimate load becomes smaller than the peak load if axial load ratio is greater than 20%. The peak and ultimate drifts decrease very quickly as the axial load ratio increases from 0% to 30%. If the axial load ratio is larger than 40%, the ultimate drift becomes less than 0.60%. The detrimental effect of axial load ratio on the ultimate drift seems to have larger impact than the ultimate drift enhancement caused by higher concrete strength and confinement. This is a very important lesson from this parametric study. Three variables have different degrees of influence on the features of backbone curve and the axial load ratio has the greatest influence.

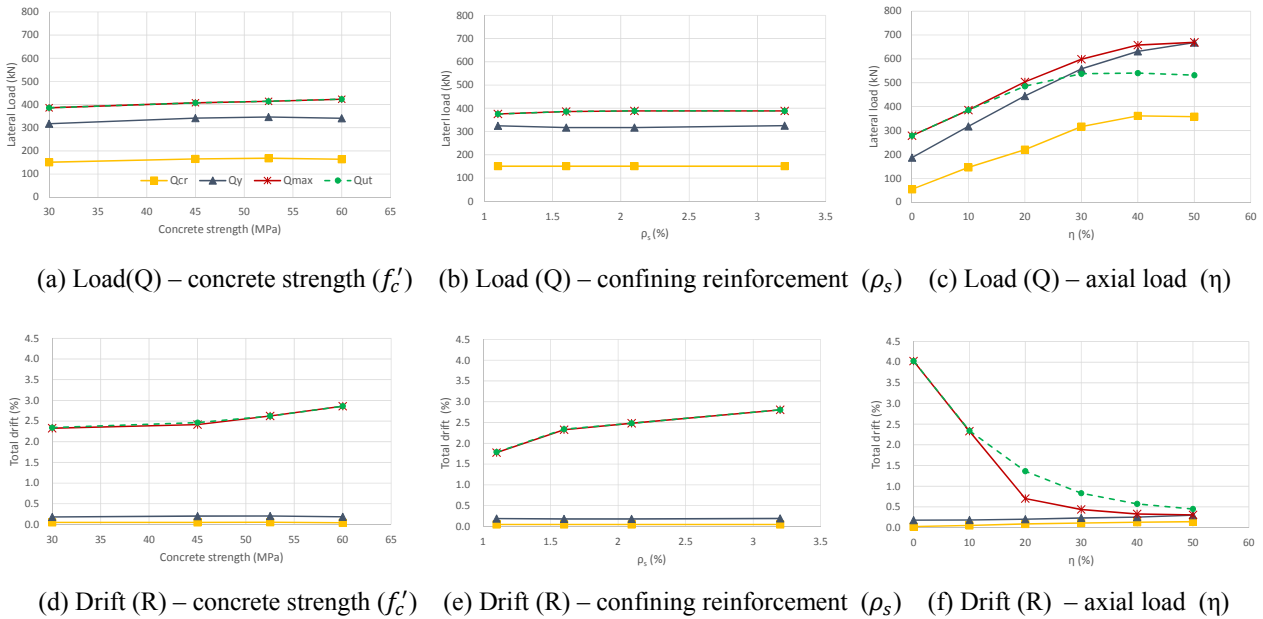


Fig. 5 – Relation of total drift, lateral load and three parameters (f'_c , ρ_s , η)

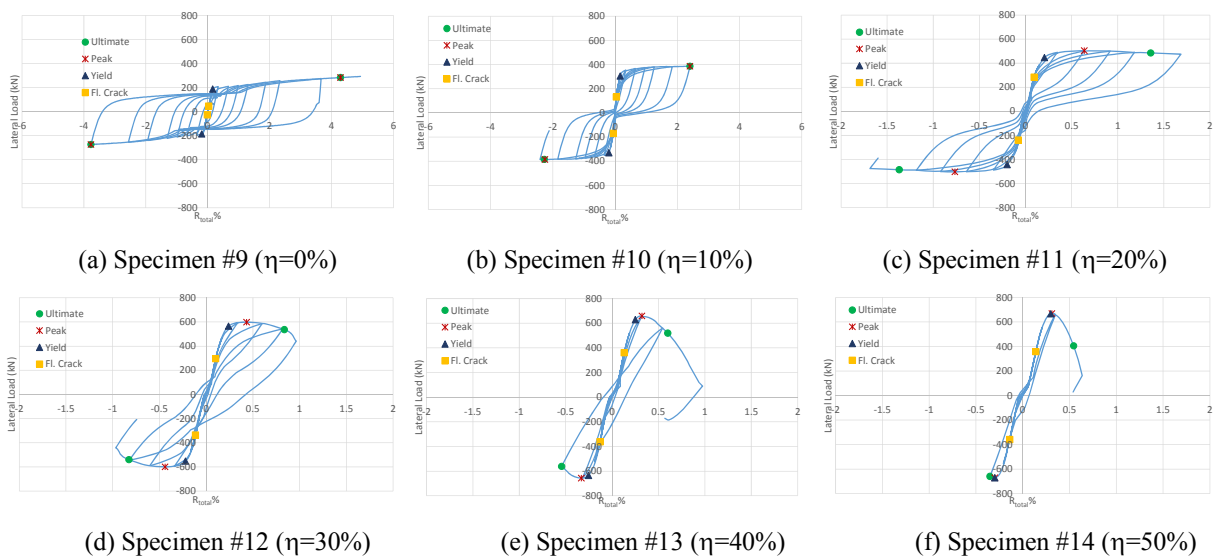


Fig. 6 – Lateral load – drift relations for specimens with various axial load ratio (η)



4. Conclusions

Parametric study was conducted on slender RC walls with a rectangular section using a fiber based computer program by choosing three important variables (concrete compressive strength, confining reinforcement ratio of boundary region and axial load ratio) to see the influence on backbone curve features.

- Axial load ratio has much more influence on backbone curve features than concrete strength and shear reinforcement ratio. Increase of axial load ratio from 0% to 50% decreases the ultimate drift capacity from 4.3% to 0.54% in this study. This large change did not happen even if concrete strength and confining reinforcement ratio were changed in ordinary range.
- Among concrete strength and confining reinforcement ratio, confining reinforcement ratio has greater influence on the ultimate drift capacity for conditions in this study.
- Drift is more sensitive to change of variables than load regarding four limit points on cracking, yielding, peak and ultimate.

5. Acknowledgements

This study was conducted as the 2015 Scientific Research B of 2015 (PI: S. Kono) and the 2016 Scientific Research A (PI: S. Kono) of JSPS Grant-in-Aid program. Some financial support was also granted by the Collaborative Research Projects of Materials and Structures Laboratory of Tokyo Institute of Technology.

6. References

- [1] Architectural Inst. of Japan (2010). "AIJ Standards for Structural Calculation of RC Structures." Architectural Inst. of Japan.
- [2] Architectural Inst. of Japan (1999). "AIJ Standards for Structural Calculation of RC Structures." Architectural Inst. of Japan.
- [3] Architectural Institute of Japan (2012). "Reconnaissance Report on The 2010 Chile Off Maule Earthquake and Reconnaissance Report on The 2011 New Zealand Christchurch Earthquake," Architectural Institute of Japan , p. 313.
- [4] Pugh, J.S., Lowes, L.N., Lehman, D.E. (2014). "Seismic Design of Slender Concrete Walls." *Proceedings of the 10th National Conference in Earthquake Engineering*, Earthquake Engineering Research Institute, Anchorage, AK.
- [5] Aaleti, S., Dai, H. and Sritharan, S. (2014). "Ductile design of slender reinforced concrete structural walls." *Proceedings of the 10th National Conference in Earthquake Engineering*, Earthquake Engineering Research Institute, Anchorage, AK.
- [6] Beyer, K., Dazio, A. and Priestley, M.J.N. (2011). "Shear Deformations of Slender Reinforced Concrete Walls under Seismic Loading." *ACI Structural Journal*, V. 108, No. 2, pp. 167-177, 2011.
- [7] Martinelli, L. (2008). "Modeling Shear-Flexure Interaction in Reinforced Concrete, Elements Subjected to Cyclic Lateral Loading." *ACI Structural Journal*, V. 105, No. 6, pp. 675-684.
- [8] Mostafaei, H. and Kabeyasawa, T. (2007). "Axial-Shear-Flexure Interaction Approach for Reinforced Concrete Columns." *ACI Structural Journal*, V. 104, No. 2, pp. 218 – 226.
- [9] Kono S., Tani M., Mukai T., Fukuyama H., Taleb R., Sakashita M. (2014). "Seismic behavior of Reinforced Concrete Walls for a performance based design." *Second European Conference on Earthquake Engineering and Seismology*, Aug 25-29, Istanbul, Turkey, ID #1471.
- [10] Kent, D. C. and Park R. (1971). "Flexural members with confined concrete" *Journal of the Structural Division, ASCE*, Vol. 97, No. 7, pp. 1969-1990.
- [11] Menegotto, M. and Pinto, P.E. (1973). "Method of analysis of cyclically loaded RC plane frames including changes in geometry and non-elastic behavior of elements under normal force and bending." *Preliminary Report IABSE*, Vol. 13.
- [12] Mander, J. B., Priestley, M. J. N., and Park, R. (1988). "Observed Stress-Strain Behavior of Confined Concrete." *Journal of Structural Engineering*, ASCE, Vol.114, No.8, August, pp. 1827-1849.
- [13] Paulay, T. and Priestley, M. J. N. (1992). "Seismic design of reinforced concrete and masonry buildings." New York, John Wiley and Sons Inc.



- [14] Kono S., Arai M., Watanabe H., Taleb R., Yuniarsyah E., Obara T., (2015). "Seismic Performance and its assessment of RC Structural Walls." *Proceeding Structural Engineering Frontier Conference*, March 18-19, 2015, Tokyo Institute of Technology, Yokohama, Japan, pp. 287-294.
- [15] ACI Committee 318, (2014). "Building Code Requirements for Structural Concrete and Commentary." The American Concrete Institute.
- [16] Kowalski, M. J. (2001). "RC structural walls designed according to UBC and displacement-based methods." *ASCE Structural Journal*, Vol. 127, No. 5, pp. 506-516.
- [17] Thomsen IV, J. H. and Wallace W. J. (2004). "Displacement-based design of slender reinforced concrete structural walls – experimental verification." *Journal of Structural Engineering*, Vol. 130, No. 4, ASCE.
- [18] Takahashi, S., Yoshida, K., Ichinose, T., Sanada, Y., Matsumoto, K., Fukuyama, H., Suwada, H. (2013). "Flexural Drift Capacity of Reinforced Concrete Wall with Limited Confinement." *ACI Structural Journal*, Vol.110, No.1, pp.95-104.
- [19] Kabeyasawa, T., Kim, Y., Sato, M., Hyunseong, H. and Hosokawa, Y. (2011). "Tests and analysis on flexural deformability of reinforced concrete columns with wing walls." *Proceedings of the Ninth Pacific Conf. on Earthquake Eng. Building an Earthquake-Resilient Society* 14-16, New Zealand, PaperID 102.
- [20] Wallace, J. W. and Moehle, J.P. (1992). "Ductility and Detailing Requirements of Bearing Wall Buildings." *J. Struct. Eng.*, 118(6), pp. 1625–1644.
- [21] Priestley, M. J. N., Seible, F., and Calvi, G. M. (1996). "Seismic design and retrofit of bridges." John Wiley and Sons Inc., New York.
- [22] Panagiorakos, T. B. and Fardis, M. N. (2001). "Deformations of reinforced concrete members at yielding and ultimate." *ACI Structural Journal*, Vol. 98, No. 2, pp. 135-148.
- [23] Bohl, A. and Adebar, P. (2011). "Plastic hinge lengths in high-rise concrete shear walls." *ACI Structural Journal*, Vol. 108, No. 2, pp. 148-157.